Superadditive and Subadditive Effects of "Hot Spot" Mutations within the Interfaces of Placental Ribonuclease Inhibitor with Angiogenin and Ribonuclease A[†]

Chang-Zheng Chen[‡,§] and Robert Shapiro*[,‡,||]

Center for Biochemical and Biophysical Sciences and Medicine and Department of Pathology, Harvard Medical School, Boston, Massachusetts 02115

Received April 1, 1999

ABSTRACT: Previous single-site mutagenesis studies on the complexes of ribonuclease inhibitor (RI) with angiogenin (Ang) and RNase A suggested that in both cases a substantial fraction of the binding energy is concentrated within one small part of the crystallographically observed interface, involving RI residues 434−438. Such energetic "hot spots" are common in protein−protein complexes, but their physical meaning is generally unclear. Here we have investigated this question by examining the detailed interactions within the RI·ligand hot spots and the extent to which they function independently. The effects of Phe versus Ala substitutions show that the key residue Tyr434 interacts with both ligands primarily through its phenyl ring; for Tyr437, the OH group forms the important contacts with RNase A, whereas the phenyl group interacts with Ang. Kinetic characterization of complexes containing multiple substitutions reveals striking, but distinctive, cooperativity in the interactions of RI with the two ligands. The losses in binding energy for the RNase complex associated with replacements of Tyr434 and Asp435, and Tyr434 and Tyr437, are markedly less than additive (i.e., by 2.4 and 1.3 kcal/mol, respectively). In contrast, the energetic effects of the 434 and 435, and 434 and 437, substitution pairs on binding of Ang are fully additive and 2.5 kcal/mol beyond additive, respectively. Superadditivities (0.9−2.4 kcal/mol) are also observed for several multisite replacements involving these inhibitor residues and two Ang residues, Arg5 and Lys40, from this part of the interface. Consequently, the decreases in binding energy for some triple-variant complexes are as large as 8.5−10.1 kcal/mol (compared to a total ΔG of −21.0 kcal/mol for the wild-type complex). Potential explanations for these functional couplings, many of which occur over distances of >13 Å and are not mediated by direct or triangulated contacts, are proposed. These findings show that the basis for the generation of hot spots can be complex, and that these sites can assume significantly more (as with Ang) or less (as with RNase) importance than indicated from the effects of single-site mutations.

The formation of tight, specific complexes between heterologous proteins is critical for most biological processes. The physicochemical basis for this molecular recognition has been investigated extensively in recent years, and substantial progress has been made (see refs *1*−*4*). Nonetheless, a predictive understanding of protein−protein interactions has not yet been achieved. The limits of our comprehension are perhaps most evident in those instances (some 20 to date; see the list in ref *5*) where binding epitopes have been defined both by crystallography and by detailed mutational studies. The structural epitopes in these complexes are invariably large and include 10−33 residues from multiple discontinuous segments on each protein. However, the functional epitopes assigned by mutagenesis are usually more restricted; replacements of a small number of amino acids (typically two to five on each protein) weaken the complex dramatically, and substitutions of most other interface residues, including many which appear to form highly favorable contacts, produce little or no loss in binding affinity.

No reliable method has been devised to pinpoint these energetic "hot spots" (*6*) by structural analysis. Indeed, these sites do not seem to share any universal characteristics that would facilitate their identification. Moreover, their physical meaning is generally unclear. For example, in most cases it is not known whether the effects of replacing critical residues can be attributed entirely to the loss of the specific interactions made by them, nor is it known whether these residues work in a cooperative manner among themselves or with other amino acids. The answers to such questions are of practical as well as theoretical interest, since they have important implications for the design of small molecules that can disrupt protein−protein interactions or functionally substitute for one of the protein components.

The complexes of RNase inhibitor (RI),[1] a 50 kDa leucine-rich repeat protein, with the ∼14 kDa members of the mammalian pancreatic RNase superfamily provide an excellent system for investigating these issues. Binding is extraordinarily tight; e.g., K_i values for the interactions of human placental RI (hRI) with human angiogenin (Ang), a ribo-

[†] This work was supported by NIH Grant HL 52096.

* To whom correspondence should be addressed: Center for Biochemical and Biophysical Sciences and Medicine, Harvard Medical School, Seeley G. Mudd Building, 250 Longwood Ave., Boston, MA 02115. Phone: (617) 432-4010. Fax: (617) 566-3137. E-mail: shapiro@ferret.med.harvard.edu.

[‡] Center for Biochemical and Biophysical Sciences and Medicine.

[§] Present address: Whitehead Institute for Biomedical Research, Massachusetts Institute of Technology, Cambridge, MA 02142.

[||] Department of Pathology.

10.1021/bi990762a CCC: $18.00
Published on Web 07/01/1999

nucleolytic enzyme that induces neovascularization (*7*, *8*), and bovine pancreatic RNase A are <1 and 40 fM, respectively (*9*). Consequently, losses of binding free energy of as much as ~12−13 kcal/mol can be quantitated, i.e., 7−8 kcal/mol beyond those which can be measured for most hormone−receptor or antigen−antibody complexes, and it is possible to accurately determine the effects of replacing multiple key residues simultaneously. The interaction of RI with Ang is of particular interest because of the essential role Ang has been shown to play in the formation of human tumors in athymic mice (*10*, *11*). Full-length hRI inhibits Ang-induced angiogenesis (*12*) and the growth of syngeneic tumors in mice (*13*), but is unlikely to be useful as an anticancer drug because of its lability, large size, and broad specificity. Knowledge of the detailed structural basis for hRI−Ang recognition might enable the development of RI derivatives with properties more suitable for therapeutic applications.

Crystal structures have been determined for the complexes of hRI with Ang (*14*) and porcine RI (pRI) with RNase A (*15*, *16*). In each case, 24 enzyme residues interact with 26−28 residues distributed widely over the inhibitor structure, which adopts a horseshoe shape formed by symmetrical arrangement of its 15 tandem repeat units (Figure 1A). The hot spot paradigm seems to apply in both instances; individual substitutions within one part of each interface decrease affinity substantially, whereas numerous replacements outside this region have no appreciable impact (*17*−*19*).

The RI residues identified as most important for interacting with Ang and RNase A are located primarily on the same short loop segment, residues 434−438 (panels B and C of Figure 1). In this study, we have explored further the roles of intermolecular contacts of these residues and the extent to which they function independently. We find that the energetic effects of various replacements within this segment on affinity for RNase A are less than additive ["subadditive" (*20*)], indicating that the binding energy within the hRI·RNase A interface may not be as concentrated as suggested by studying the single-site variants. In contrast, the effects of eliminating contacts of residues 434−438 with Ang are largely additive or beyond additive ("superadditive"). Thus, this segment may assume even greater importance for Ang binding than was first apparent. These results show that the basis for the generation of hot spots can be varied and complex, and emphasize the need to move beyond single-site mutagenesis in determining the distribution of binding free energy within protein−protein interfaces.

EXPERIMENTAL PROCEDURES

Materials. Primers were synthesized by Genosys or Promega. CpA and CpG were purchased from Sigma. RNase A (type RAF) and bovine serum albumin (RNase-free) (BSA) were obtained from Worthington. Human Ang (both the native <Glu1 form and the Met−1/Gln1 derivative), [^{14}C-(U)]Ang (2700 cpm/μg), the Ang variants R5A, K40G, and W89M, hRI, and the hRI variants Y434A, D435A, and Y437A were produced in *Escherichia coli* as described previously (*18*, *19*, *21*, *22*). <Glu1 and Met−1/Gln1 Ang have identical rate constants for dissociation from hRI (*23*) and were used interchangeably for dissociation experiments. Association rate constants for the two proteins differ somewhat; only the <Glu1 form was employed for measuring this parameter. RNase A− and Ang−Sepharose were prepared by the method of Blackburn et al. (*24*). Buffers used for kinetic experiments were degassed prior to being used.

Determination of Protein Concentrations. Concentrations of RNase A, Ang, and the Ang variants R5A and K40G were determined spectrophotometrically [for RNase A, $\epsilon_{278} = 9800$ M^{-1} cm^{-1} (*25*); for Ang, $\epsilon_{280} = 12500$ M^{-1} cm^{-1}]; W89M-Ang was quantitated by amino acid analysis. Concentrations of hRI and all single-residue hRI variants were based on measurements of inhibition of RNase A activity (*26*). The hRI double mutants Y434A/D435A and Y434A/Y437A were quantitated by the Bradford method (Bio-Rad); the standard was a sample of hRI [in 20 mM Hepes (pH 7.6)] which was itself quantitated spectrophotometrically [$\epsilon_{281} = 45\,000$ M^{-1} cm^{-1} (F. S. Lee and R. Shapiro, unpublished)].

Site-Directed Mutagenesis and Production of Variant Proteins. Fragments of hRI cDNA containing the desired mutations were generated by overlap extension PCR (*27*) with *Pfu* DNA polymerase (Stratagene). The template was the expression plasmid pTRP-PRI (*21*); the external flanking primers were 5′-GGTGTGACATCAGACAACTGC-3′ [nucleotides 749−769 in the hRI cDNA sequence (*28*)] and 5′-TCGACGGATCCCCGGGAATTC-3′ (from the 3′-noncoding region of the plasmid), and the internal mutagenic primers were 5′-GCTGGTCCTGTTTGACATTTACTGG-3′ and 5′-AGTAAATGTCAAACAGGACCAGCTG-3′ (Y434F), 5′-GTACGACATTTTTTGGTCTGAGGAG-3′ and 5′-CCTCAGACCAAAAAATGTCGTACAG-3′ (Y437F), 5′-CTGGTCCTGGCTGCTATTTACTGGTCTGAGGAG-3′ and 5′-CCAGTAAATAGCAGCCAGGACCAGCTGCTCCAGG-3′ (Y434A/D435A), and 5′-GCTGGTCCTGGCTGACATTGCTTGGTCTGAGGAGATGG-3′ and 5′-CCTCAGACCAAGCAATGTCAGCCAGGACCAGCTGCTCC-3′ (Y434A/Y437A). The final PCR products were digested with *Stu*I and *Eco*RI and ligated into pTRP-PRI that had been cleaved with the same enzymes. DNA sequencing of PCR-amplified regions in all cases confirmed the presence of the intended mutations and the absence of any spurious changes. Variants were expressed in *E. coli* strain W3110 cells transformed with the mutant plasmids and were purified by ammonium sulfate precipitation and chromatography on RNase A−Sepharose (*29*) or Ang−Sepharose (*19*). The final products were dialyzed into 20 mM Hepes (pH 7.6) containing 50 mM KCl, 8 mM DTT, 1 mM EDTA, and 50% glycerol and stored at −20 °C. Yields were ~200 μg per liter of culture. SDS−PAGE analysis revealed that all variants were >95% homogeneous and were the same size as the native proteins. The amino acid compositions of all proteins were consistent with their proposed structures.

Kinetics. (A) Assays. The enzymatic activity of RNase A was measured spectrophotometrically with 75 μM CpA or CpG as the substrate (*30*) in buffer A [0.1 M Mes (pH 6.0) containing 0.1 M NaCl and 1 mM EDTA] and 10 μg/mL

[1] Abbreviations: RI, ribonuclease inhibitor; hRI, human placental ribonuclease inhibitor; Ang, angiogenin; RNase A, bovine pancreatic ribonuclease A; pRI, porcine ribonuclease inhibitor; CpA, cytidylyl-(3′→5′)adenosine; CpG, cytidylyl-(3′→5′)guanosine; BSA, bovine serum albumin; Mes, 2-(*N*-morpholino)ethanesulfonic acid; SE, standard error.

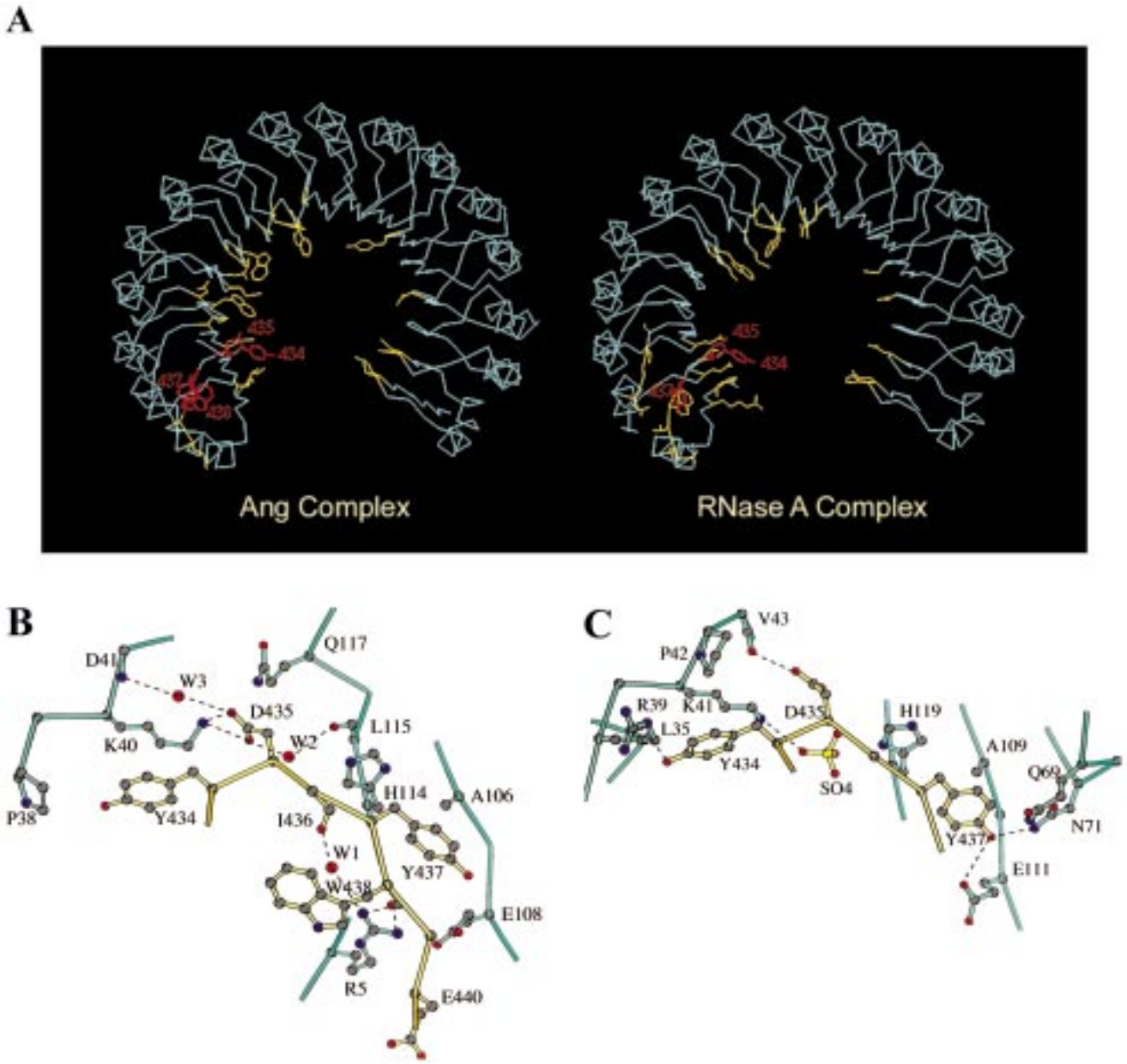

FIGURE 1: (A, left) Crystal structure of hRI in its complex with Ang (*14*), showing the α-carbon backbone and side chain atoms of the contact residues. Hot spot residues Tyr434, Asp435, Tyr437, and Trp438 are red; other contact residues are yellow. (A, right) Crystal structure of pRI in its complex with RNase A (*15*, *16*), showing the α-carbon backbone and side chain atoms of the contact residues. Hot spot residues Tyr434, Asp435, and Tyr437 (hRI numbering) are red; other contact residues are yellow. (B) Details of the interactions between hRI residues 434−438 (yellow) and Ang (cyan) in the crystal structure, with oxygen atoms in red and nitrogen atoms in blue. H-bonds are denoted by dashed lines. Water molecules are labeled W1, W2, and W3. (C) Details of the interactions between hRI Tyr434, Asp435, and Tyr437 (yellow) and RNase A (cyan), based on the crystal structure of the pRI·RNase A complex, with oxygen atoms in red and nitrogen atoms in blue. H-bonds are denoted by dashed lines. Part A was drawn with Quanta (Molecular Simulations). Parts B and C were drawn with MOLSCRIPT (*53*).

BSA at 25 °C. The RNase A concentrations were 0.2−0.3 and 3 nM for assays with CpA and CpG, respectively.

(B) Dissociation Rate Constants. Dissociation rate constants for Y434F-hRI· and Y437F-hRI·ligand complexes were determined by adding to the complex a scavenger for free inhibitor and then measuring the amount of free ligand present at various times (*9*, *19*). Incubations were performed at 25 °C in buffer A, DTT (5 mM with RNase A and 120 μM with Ang), and 100 μg/mL BSA. For incubations with RNase A (20 nM), the scavenger was Ang (10 μM), and quantitation of free RNase A was based on the activity of 10−15 μL aliquots toward CpA. The activity of Ang in this assay is undetectable. For Ang·inhibitor complexes, ^{14}C-labeled ligand (0.9−1.4 μM) was used and the scavenger was unlabeled Ang (20 equiv). Bound and free [^{14}C]Ang in 70−140 μL aliquots of these mixtures were separated by Mono S cation-exchange chromatography and quantitated by scintillation counting. Elution was achieved with a 15 min linear gradient from 0.2 to 0.6 M NaCl in 10 mM Tris (pH 8) at a flow rate of 1.5 mL/min. As for previous complexes (see ref *19*), dissociation was biphasic, with a relatively rapid release of some ligand (16−20% for RNase A and 2−3% for Ang), followed by a slower dissociation of the remainder. Data for the slower phase (six to nine points per complex) were fitted to a single-exponential decay process with SigmaPlot 4.0 (SPSS) to obtain k_d. Dissociation

of RNase A complexes was followed for one or two half-lives; experiments with Ang complexes were conducted over 8 days, during which 7−10% dissociation occurred.

Dissociation of other Ang complexes and all complexes of Ang variants was monitored by fluorescence spectroscopy (see below). Incubations were performed in buffer A at 25 °C. Ten minutes after formation of the complex (each component at 0.1 μM), 1−2 μM W89M-Ang was added as a scavenger for free hRI or the hRI variant, and the decrease in Trp fluorescence (see the Results) was followed for at least six half-lives. Data were fitted to a single-exponential decay as described above.

(C) Association Rate Constants. Association of hRI and its derivatives with Ang and Ang variants was assessed by using the stopped-flow fluorimeter to monitor the enhancement in Trp fluorescence that accompanies complex formation (*26*). The conditions were the same as for dissociation experiments, except that the DTT concentration was 25−50 μM and BSA was not added. The inhibitor concentration was 50 nM. Association of wild-type Ang complexes was assessed at four or five concentrations of Ang ranging from 0.25 to 1.5 μM (i.e., under pseudo-first-order conditions in all cases); between seven and eleven replicates were recorded at each concentration, and more than five half-lives of the reaction were used for analysis. Association of the complexes of Ang variants was examined at a single concentration (100 nM for R5A and 150 nM for K40G); five or six replicate measurements were taken, and only the first half-life was used for data analysis to minimize any error due to ligand depletion. The fluorescence increases were fitted to a single- or double-exponential decay equation to obtain values of k_{obs}; for biphasic association, k_{obs} represents the faster rate constant (see the Results). Data for complexes of wild-type Ang were plotted as $1/k_{obs}$ versus 1/[Ang] and fitted by linear regression; the slope equals $1/k_a$, where k_a is the apparent second-order rate constant of association (*26*). The k_a values for complexes of Ang variants represent k_{obs} divided by the ligand concentration. Values of k_a for RNase A−inhibitor complexes were determined from the rate constants for the corresponding Ang complexes by measuring the competition between the two ligands for inhibitor in a spectrophotometric assay of RNase A activity toward CpG (*26*).

(D) Dissociation Constants. K_i values for all Ang and Ang variant complexes and for the complexes of RNase A with Y434F-hRI and Y437F-hRI were calculated from the rate constants for dissociation and association ($K_i = k_d/k_a$). K_i values for the complexes of RNase A with the hRI double mutants Y434A/D435A and Y434A/Y437A were obtained by measuring enzymatic activity toward CpA in the presence of five to seven concentrations of inhibitor and performing nonlinear fits of the data to the equation $v_i = v_0/(1 + [I]/K_i)$ with SigmaPlot 4.0, where v_i and v_0 are initial velocities in the presence and absence of inhibitor, respectively, and [I] is the inhibitor concentration; the concentration of CpA was well below K_m. A K_i value for the complex of Y434A/D435A-hRI with Ang was also determined from that for the RNase A complex by measuring the competition between the two ligands fluorimetrically. This method is based on the 1.5-fold difference in the Trp fluorescence emission level between the Ang·RI and RNase A·RI complexes (*26*). Spectra of mixtures of 100 nM inhibitor, 150 nM Ang, and 4.5 or 12.4 μM RNase A in buffer A were recorded after incubation for 45 min at 25 °C; this amount of time is >10 half-lives of dissociation for the two complexes and is therefore sufficient for reaching equilibrium. The distributions of inhibitor between the two enzymes were then determined by reference to spectra of mixtures of 100 nM inhibitor with either 150 nM Ang or 8.9 μM RNase A using the emission intensity at 360 nm. The K_i value for the Ang complex equals the K_i value for the RNase complex multiplied by $[A]_F[R]_B/[R]_F[A]_B$, where A and R refer to Ang and RNase A, respectively, and B and F refer to bound and free, respectively.

(E) Propagation of Standard Error. Standard errors (SEs) for K_i values equal K_i times the square root of the sum of the squares of fractional SEs for k_d and k_a. SEs for values of ΔG ($=RT \ln K_i$) equal RT times the fractional SE for K_i. SEs for values of $\Delta\Delta G$ [the difference between ΔG values for wild-type (wt) and variant (var) complexes] are the square root of the sum of the squares of SEs for ΔG_{wt} and ΔG_{var}. SEs for values of $\Delta\Delta\Delta G$ (the difference between the sum of the $\Delta\Delta G$ values for the single-residue variants and the observed $\Delta\Delta G$ value for a multiple-residue variant) are the square root of the sum of the squares of SEs for $\Delta\Delta G$ values for the multiple-residue variant complex and the single-residue variant complexes. The calculated SEs in $\Delta\Delta G$ for all complexes examined here are <0.2 kcal/mol, and in all but three instances are <0.1 kcal/mol; errors for earlier complexes (not reported previously) are ≤0.1 kcal/mol. SEs for all $\Delta\Delta\Delta G$ values are ≤0.2 kcal/mol.

Fluorescence Measurements. Fluorescence spectra were measured with a Jobin Yvon-Spex FluoroMax-2 fluorimeter. Excitation was at 285 nm, and emission was recorded from 300 to 400 nm, except in the competition experiment where excitation was at 295 nm to minimize any contribution of RNase A tyrosines, and emission was monitored between 340 and 400 nm. Time-based data acquisition on this instrument was performed at 2.5 s intervals with excitation at 285 nm (0.7 nm slit) and emission at 365 nm (25 nm slit). Stopped-flow measurements were performed with an Applied Photophysics instrument. Excitation was at 285 nm (2 nm slit), and emission was monitored with a 340 nm band-pass filter; 2000 data points were collected for each experiment.

RESULTS

Rationale for the Mutational Studies. In the crystal structure of the hRI·Ang complex, the side chains of hRI residues Tyr434, Asp435, and Tyr437 and the main chain of hRI Trp438 contact Arg5, Lys40, Ala106, Glu108, His114, and Gln117 of Ang (Figure 1B and Table 1). Replacements of Asp435 and Arg5 with Ala and Lys40 with Gln were shown previously to decrease affinity markedly; these effects can potentially be understood as consequences of eliminating the H-bonds of Asp435 with Lys40 and Trp438 with Arg5. The relatively minor change associated with the substitution of Tyr437 with Ala also seems reasonable, since this residue only makes five van der Waals contacts with Ang. In contrast, replacement of Tyr434 by Ala, which also removes only a relatively small number of van der Waals interactions, produces a large reduction in complex stability.

The Tyr434 mutation decreases the affinity for RNase A even more substantially than for Ang; indeed, the loss in

Table 1: Effects of Previous Single-Residue Replacements within the Hot Spot Region of the hRI−Ang and hRI−RNase A Interfaces

replacement	$K_{i,var}/K_{i,wt}$[a] [$\Delta\Delta G$[b] (kcal/mol)]	intermolecular contacts eliminated in the crystal structure[c]
Effects on Ang Binding		
hRI Tyr434 → Ala	246 (3.3)	6 van der Waals contacts with Lys40 (CG−CE, CD1−CE, CD1−CD, CE1−CD, CD2−CG, and CE2−CB)[d]
hRI Asp435 → Ala	358 (3.5)	2 H-bonds with Lys40 [OD1···NZ (2.9 Å) and OD2···NZ (3.0 Å)] 2 water-mediated H-bonds[e] [OD1···O of Leu115 (2.6 Å/2.9 Å), OD2···N of Asp41 (3.3 Å/3.3 Å)] 7 van der Waals contacts with Lys40 (CG−CE, CG−NZ, and OD1−CE) and Gln117 (CG−CB, CG−CG, OD1−CG, and OD2−CG)
hRI Tyr437 → Ala	4.1 (0.8)	5 van der Waals contacts with Ala106 (CD1−CB and CE1−CB), Glu108 (OH−OE2), and His114 (CD1−CB and CD1−CG)
Ang Arg5 → Ala	50 (2.3)	2 H-bonds with Trp438 [O···NH1 (3.2 Å) and O···NH2 (2.6 Å)] 1 water-mediated H-bond [I436 O···NH2 (3.2 Å/2.8 Å)] 6 van der Waals contacts with Trp438 (O−CZ, CD1−NH2, and C−NH2), Ser439 (C−NH1), and Glu440 (CA−NH1 and CG−CD)
Ang Lys40 → Gln	1300 (4.2)	H-bonds of NZ with Asp435; van der Waals contacts of NZ and CE with Tyr434 and Asp435 (see above)
Effects on RNase A Binding[f]		
hRI Tyr434 → Ala	23000 (5.9)	1 H-bond with Leu35 [OH···O (3.4 Å)] 13 van der Waals contacts with Arg39 (OH−O, CE2−CG, and CE2−CD), Lys41 (CZ−CA, CE2−CA, CG−CG, CE1−CB, CE1−CG, CE1−CD, CD1−CG, and CD1−CD), and Pro42 (CG−CD and CD2−CD)
hRI Asp435 → Ala	470 (3.6)	1 H-bond with Val43 [OD2···O (3.2 Å)][g] 1 van der Waals contact with Lys41 (OD2−CE)
hRI Tyr437 → Ala	84 (2.6)	2 H-bonds with Asn71 [OH···ND2 (2.7 Å)] and Glu111 [OH···OE1 (3.2 Å)] 13 van der Waals contacts with Gln69 (CD2−NE2 and CE2−NE2), Asn71 (OH−CG, CZ−ND2, CE2−OD1, and CE2−ND2), Ala109 (CZ−CB and CE2−CB), Glu111 (OH−CG, OH−CD, CZ−OE1, and CE1−OE1), and His119 (CG−CD2)

[a] The K_i for the variant protein divided by the K_i for the wild-type protein. Effects of replacements are from refs *17*−*19*. [b] $\Delta\Delta G$ values are the differences in binding free energies for wild-type and variant complexes, calculated from the equation $\Delta\Delta G = -RT \ln(K_{i,wt}/K_{i,var})$. [c] The reference structures are 1A4Y [hRI·Ang (*14*)] and 1DFJ [pRI·RNase A (*15*)]. The contacts of hRI with RNase A are assumed to be the same as for pRI. The interactions that are listed were assigned using criteria specified in the respective publications; distance cutoffs were somewhat shorter for the Ang complex, which was of higher resolution (2.0 vs 2.5 Å). Distances are listed only for H-bonds. [d] Contacts are listed with the hRI atom first and the Ang or RNase A atom second. [e] Water-mediated H-bonds are listed with the hRI−water distance first and water−Ang distance second. [f] RNase A and Ang residue equivalents are as follows: Leu35 and Leu35, Arg39 and Pro38, Lys41 and Lys40, Pro42 and Asp41, Val43 and Ile42, Ala109 and Ala106, Glu111 and Glu108, and His119 and His114; no Ang residues correspond structurally to Gln69 and Asn71 in RNase A. [g] The interactions of Asp435 in the RI·RNase A crystal structure most likely differ from those present under the conditions used for kinetic characterization. (i) The H-bond with Val43 would not be present if the Asp carboxyl group is unprotonated, as expected, and (ii) Asp435···Lys41 H-bonds of the type observed in the Ang complex are probably formed (see the text).

binding free energy ($\Delta\Delta G$) of 5.9 kcal/mol is by far the largest for any substitution in the three proteins. The side chain of residue 434 forms more extensive interactions with RNase A (one H-bond and 13 van der Waals contacts; Table 1 and Figure 1C) than with Ang. However, replacement of Tyr437 eliminates a similar number of interactions and yet produces a much more modest change in binding strength, 2.6 kcal/mol. [The interactions cited are those in the pRI·RNase A complex and are assumed to be present in the hRI complex as well: the K_i values for the two complexes are indistinguishable (*9*, *31*), the sequences of hRI (*28*) and pRI (*32*) are 77% identical, and the region under examination is especially well-conserved.] Substitution of Asp435 in hRI destabilizes the complex with RNase A to the same degree as that with Ang, suggesting that similar interactions have been eliminated. Although the pRI·RNase A crystal structure exhibits no H-bonds corresponding to those of Asp435 with Lys40 in the Ang complex (the analogous lysine, Lys41, instead binds a sulfate ion from the crystallization medium), such interactions probably form under the conditions used for kinetic characterization, where sulfate and similar anions are not present (*14*); this would require only a slight reorientation of the ϵ-amino group of Lys41 to a position already observed for it in some crystal structures of the free enzyme (*33*).

The preceding observations raise numerous questions regarding the interactions of the hRI segment of residues 434−438 with Ang and RNase A, particularly with respect to the structural bases for the dramatic losses in affinity associated with replacement of Tyr434. What is the relative importance of H-bonds versus van der Waals contacts and the hydrophobic effect in the interactions of Tyr434 and Tyr437 with RNase A? Does Tyr434 form contacts with either enzyme that are not apparent from the crystal structures? Does the Tyr434 mutation disrupt contacts of other hRI residues? More generally, are the functional effects of replacing the individual interface residues independent? We initially addressed these questions by characterizing the complexes of RNase A and Ang with four new hRI variants: Y434F, Y437F, Y434A/D435A, and Y434A/Y437A. Interrelationships within this region of the hRI·Ang interface were then investigated further through kinetic studies on the complexes of R5A-Ang and K40G-Ang with hRI single and double mutants.

Interactions of Y434F-hRI and Y437F-hRI with RNase A and Ang. The hRI variants Y434F and Y437F were produced

Table 2: Kinetic Constants for the Complexes of hRI Variants Y434F and Y437F[a]

hRI	ligand	k_d (s^{-1})	k_a (M^{-1} s^{-1})	K_i (M)	$K_{i,var}/K_{i,wt}$	$\Delta\Delta G^b$ (kcal/mol)
wild-type[c]	RNase A	$(1.2 \pm 0.1) \times 10^{-5}$	$(3.8 \pm 0.6) \times 10^{8}$	$(3.1 \pm 0.5) \times 10^{-14}$	–	–
Y434F	RNase A	$(1.0 \pm 0.1) \times 10^{-5}$	$(2.6 \pm 0.1) \times 10^{8}$	$(3.8 \pm 0.4) \times 10^{-14}$	1.2	0.1
Y437F	RNase A	$(2.9 \pm 0.1) \times 10^{-4}$	$(2.5 \pm 0.2) \times 10^{8}$	$(1.2 \pm 0.1) \times 10^{-12}$	39	2.1
wild-type[c]	Ang	$(1.1 \pm 0.2) \times 10^{-7}$	$(2.8 \pm 0.2) \times 10^{8}$	$(3.9 \pm 0.8) \times 10^{-16}$	–	–
Y434F	Ang	$(1.6 \pm 0.1) \times 10^{-7}$	$(1.6 \pm 0.2) \times 10^{8}$	$(1.0 \pm 0.1) \times 10^{-15}$	2.6	0.6
Y437F	Ang	$(9.0 \pm 1.0) \times 10^{-8}$	$(1.5 \pm 0.1) \times 10^{8}$	$(5.9 \pm 0.8) \times 10^{-16}$	1.5	0.2

[a] Kinetic parameters were determined as described in Experimental Procedures. [b] Standard errors for all $\Delta\Delta G$ values are $\leq$0.1 kcal/mol. [c] Kinetic parameters for wild-type hRI·RNase A and hRI·Ang complexes are from ref *19*; ΔG values are -18.4 ± 0.1 and -21.0 ± 0.1 kcal/mol, respectively. The errors listed were not reported previously. Values measured at the same time as those for variant complexes did not differ significantly.

Table 3: Kinetic Constants for the Complexes of hRI Variants Y434A/D435A and Y434A/Y437A with Wild-Type RNase A and Ang[a]

hRI	ligand	k_d (s^{-1})	k_a (M^{-1} s^{-1})	K_i (M)	$K_{i,var}/K_{i,wt}$	$\Delta\Delta G^b$ (kcal/mol)	$\Delta\Delta\Delta G^c$ (kcal/mol)
Y434A/D435A	RNase A	–	–	$(5.6 \pm 0.3) \times 10^{-9}$	181 000	7.1	2.4
Y434A/Y437A	RNase A	–	–	$(6.3 \pm 0.9) \times 10^{-9}$	203 000	7.2	1.3
Y434A/D435A	Ang	$(2.7 \pm 0.4) \times 10^{-3}$	$(7.0 \pm 0.3) \times 10^{7}$	$(3.9 \pm 0.6) \times 10^{-11}$	100 000	6.8	0
Y434A/Y437A	Ang	$(1.7 \pm 0.1) \times 10^{-3}$	$(5.9 \pm 0.3) \times 10^{7}$	$(2.9 \pm 0.2) \times 10^{-11}$	74 400	6.6	−2.5

[a] Kinetic parameters were determined as described in Experimental Procedures. Values for the wild-type complexes are listed in Table 2. [b] Standard errors for all $\Delta\Delta G$ values are <0.15 kcal/mol. [c] Sum of $\Delta\Delta G$ values for single-residue variants (see Table 1) minus the $\Delta\Delta G$ value for the double mutant. Standard errors for $\Delta\Delta\Delta G$ values are all $\leq$0.2 kcal/mol.

in *E. coli* and purified to homogeneity by RNase A−Sepharose chromatography. Kinetic analysis of their interactions was performed by standard methods (see Experimental Procedures), and K_i values were calculated from the rate constants for dissociation (k_d) and association (k_a). Replacement of Tyr434 by Phe had essentially no effect on binding of RNase A (Table 2), indicating that the putative H-bond of this residue does not contribute to complex stability and that the attenuated affinity of Y434A is due only to the loss of the phenyl group. In contrast, replacement of Tyr437 by Phe weakened the hRI·RNase A interaction almost to the same extent (2.1 kcal/mol) as had substitution with Ala (2.6 kcal/mol). Thus, the OH group rather than the phenyl ring of this Tyr appears to provide the energetically important interactions.

The Tyr434 → Phe substitution decreased the binding energy of the Ang complex by 0.6 kcal/mol (vs 3.3 kcal/mol for the Ala replacement), suggesting that this residue again participates primarily through its phenyl ring, but that the OH group may play a minor role as well. Replacement of Tyr437 with Phe did not alter the affinity significantly, consistent with the absence of any H-bond for this residue in the three-dimensional structure.

Interactions of Y434A/D435A-hRI and Y434A/Y437A-hRI with RNase A. Recombinant Y434A/D435A and Y434A/Y437A hRIs were prepared in the same manner as the other variants, except that Ang−Sepharose was used for the final purification step (*19*). Binding constants for the complexes of these variants with RNase A were determined directly by measuring the extent of inhibition of enzymatic activity, as had been done previously with Y434A; indeed, dissociation was too rapid to allow measurement of k_d and k_a by available methods. Both hRI mutants bound only 8−9-fold less tightly than the single Y434A derivative. Thus, the impacts of the double replacements (Table 3) were 59-fold (Y434A/D435A) and 10-fold (Y434A/Y437A) smaller than would be expected if the individual substitutions reduce the affinity by independent mechanisms. In energetic terms, the effects of the replacements are subadditive; the difference ($\Delta\Delta\Delta G$) between the sum of $\Delta\Delta G$ values for the single-residue variants and the measured $\Delta\Delta G$ value for the double-mutant complex is 2.4 kcal/mol for the 434 and 435 pair and 1.3 kcal/mol for the 434 and 437 pair.

Interactions of Y434A/D435A-hRI and Y434A/Y437A-hRI with Angiogenin. Attempts to measure K_i values for the complexes of Ang with the hRI double mutants by the standard method were unsuccessful because neither complex remained intact during the chromatographic procedure that was used to quantitate bound and free Ang in dissociation experiments. Thus, it was necessary to develop an alternative approach for determining affinity. The ribonucleolytic activity of Ang is extremely weak (*8*), precluding measurement of K_i by enzymatic assay. Instead, a fluorescence-based technique for monitoring dissociation was devised. Lee and co-workers had demonstrated that the fluorescence of the complex of Ang (which contains a single tryptophan, at position 89) and hRI (with six Trps) is twice that of the oxindolylalanine-89−Ang complex (*26*), and that Trp-oxidized Ang binds almost as tightly as the wild-type protein (*17*). These findings suggested that k_d values for the complexes of Ang with Y434A/D435A-hRI and Y434A/Y437A-hRI could be determined by adding to the complexes excess Trp-modified Ang and then following the decrease in fluorescence as the inhibitor dissociates from Ang and binds to the Ang derivative. The feasibility of this approach was tested with the Ang variant W89M (*22*) rather than with the oxidized protein, which is more difficult to prepare.

Met substitution of Trp89 had no significant effect on complex stability (results not shown). Addition of W89M-Ang to wild-type hRI produced a several-nanometer blue shift in the fluorescence emission spectrum; the maximum was 10% lower than that for hRI itself (Figure 2). Addition of a 10-fold molar excess of this protein to the Ang·Y434A/D435A-hRI complex induced a ~30% decrease in fluorescence emission that occurred with a half-life of 4.3 min (Figure 3), i.e., 24400-fold faster than for the wild-type complex ($t_{1/2}$ = 73 days) (Table 3). Dissociation of the Ang·

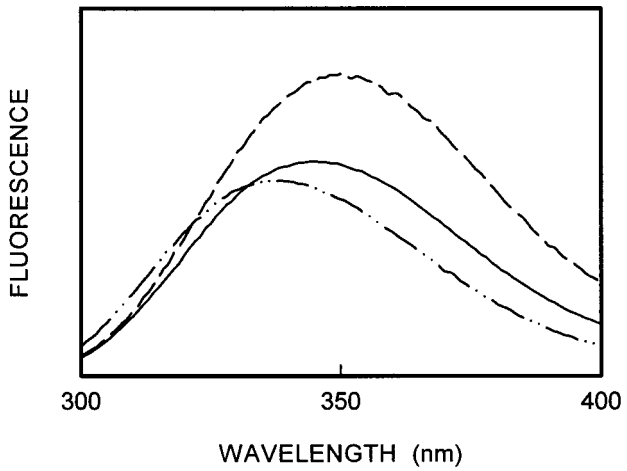

FIGURE 2: Fluorescence emission spectra of hRI (—) and the complexes of hRI with Ang (— —) and W89M-Ang (—••—). All protein concentrations were 0.1 μM in 0.1 M Mes (pH 6.0) containing 0.1 M NaCl and 1 mM EDTA at 25 °C. Excitation was at 285 nm.

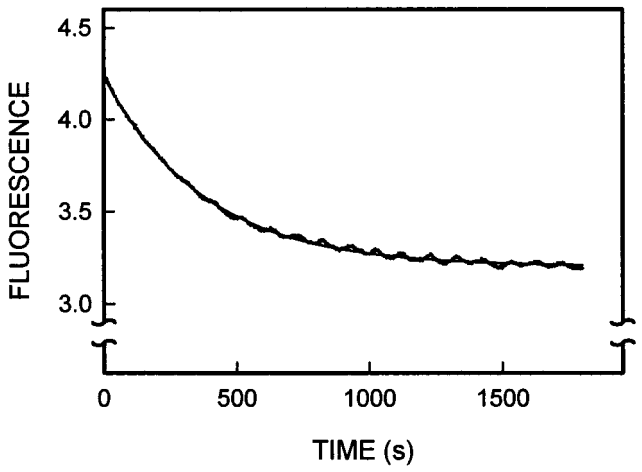

FIGURE 3: Dissociation of the complex of Ang with Y434A/D435A-hRI, as measured by the decrease in fluorescence after addition of W89M-Ang as a scavenger for free inhibitor. The line represents the best fit of the data to a three-parameter equation for exponential decay.

Y434A/Y437A-hRI complex was accelerated almost as much, by a factor of 16 000.

The effects of the hRI double mutations on association were investigated by the standard stopped-flow fluorimetric method with a fixed concentration of inhibitor and multiple concentrations of Ang ranging from a 4- to a 30-fold molar excess. In all instances, the fluorescence increase that accompanied complex formation was markedly biphasic (see Figure 4), whereas a single-exponential process had been observed for the wild-type complex and for every variant complex examined previously. The data fit well to a double-exponential equation, with rate constants for the two processes differing by a factor of at least 6 at all Ang concentrations.

Because of the unusual association behavior, it was not immediately apparent how to obtain values for k_a from the stopped-flow data. This calculation is straightforward for the wild-type complex, where association of Ang (E) and hRI (I) occurs by a two-step kinetic mechanism in which rapid formation of a loose complex EI (dissociation constant K_1 = 0.3 μM) is followed by a slower isomerization to the tight

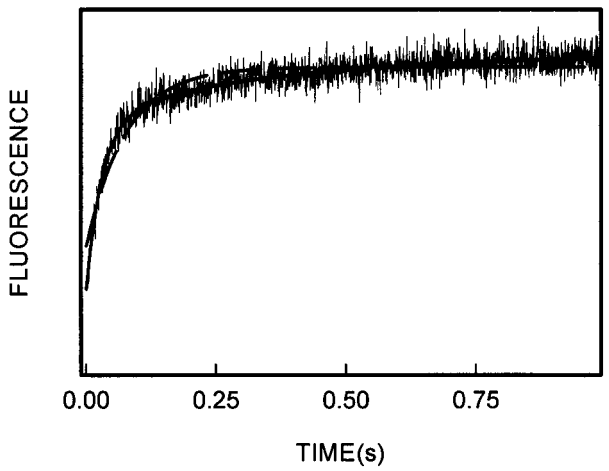

FIGURE 4: Association of the complex of Ang (500 nM) with Y434A/Y437A-hRI (50 nM) as monitored by fluorescence. The dashed line represents the best fit of the data to a single-exponential process; the solid line is the best fit to a double-exponential process.

complex EI* (rate constant k_2 = 80 s^{-1}) (*26*; values cited are from ref *19*). The initial E + I $\rightleftarrows$ EI equilibrium for the wild-type complex is established within the dead time of the instrument (<1 ms), and the subsequent fluorescence change, which is a single-exponential process, reflects conversion of EI and remaining E + I to EI*. The rate constant for this process, k_{obs}, equals $k_{-2} + k_2$[Ang]/(K_1 + [Ang]) (k_{-2} is the rate constant for the reverse isomerization and can be ignored for most complexes); k_a equals k_2/K_1 and is determined from the dependence of k_{obs} on Ang concentration (see Experimental Procedures). For the hRI double mutants, the calculation is less straightforward. One obvious potential explanation for the biphasic association of the complexes of these variants is that the amino acid replacements have prolonged the first step to the point where it is observable. In this case, the slower of the two processes would correspond to the single phase seen with the wild-type complex. Alternatively, the faster process might correspond to that normally measured (i.e., EI → EI*), with formation of EI still taking place during the dead time and the slower phase reflecting an additional step in the inhibition mechanism or an experimental artifact.

Values for k_a determined on the basis of these two interpretations differ substantially. Three considerations, taken together, strongly support the latter view and indicate that k_a can be calculated by treating the rate constant for the faster process as k_{obs} in the standard procedure. (1) Most of the fluorescence increase with the wild-type complex is due to the conversion of EI to EI* rather than to formation of EI (R. Shapiro, unpublished results); between 70 and 85% of the fluorescence increase with the double mutants is associated with the faster process. (2) The dependence of the faster rate constant on Ang concentration for Y434A/D435A is linear over the entire range of concentrations examined, reaching a value of 105 s^{-1} at 1.5 μM Ang. If these rates reflect EI → EI*, then both K_1 and k_2 are much larger than for wild-type hRI (see above), as was the case for the Y434A and D435A single-residue variants (*19*). However, if the faster rate constants reflect E + I $\rightleftarrows$ EI, then k_2, as derived from data for the slower phase, would be considerably smaller than for wild-type inhibitor (K_1 would be unchanged); i.e., the effect of the double substitution on k_2 would be the opposite of that for the single replacements. (3) An ap-

Table 4: Kinetic Constants for the Complexes of R5A-Ang and K40G-Ang with hRI and hRI Variants[a]

Ang	hRI	k_d (s^{-1})	$t_{1/2}$	k_a (M^{-1} s^{-1})	K_i (M)	$\Delta\Delta G^b$ (kcal/mol)	$\Delta\Delta\Delta G^c$ (kcal/mol)
R5A	Y434A	$(2.8 \pm 0.1) \times 10^{-3}$	4.2 ± 0.2 min	$(5.5 \pm 0.2) \times 10^{7}$	$(5.1 \pm 0.2) \times 10^{-11}$	7.0	−1.4
R5A	D435A	$(2.7 \pm 0.3) \times 10^{-3}$	4.4 ± 0.4 min	$(7.6 \pm 0.2) \times 10^{7}$	$(3.6 \pm 0.4) \times 10^{-11}$	6.7	−0.9
R5A	Y434A/D435A	$(6.2 \pm 0.3) \times 10^{-1}$	1.1 ± 0.1 s	$(6.2 \pm 0.2) \times 10^{7}$	$(1.0 \pm 0.1) \times 10^{-8}$	10.1	−1.0
R5A	Y434A/Y437A	$(2.8 \pm 0.6) \times 10^{-2}$	25 ± 6 s	$(4.0 \pm 0.2) \times 10^{7}$	$(7.0 \pm 1.5) \times 10^{-10}$	8.5	−2.1
K40G	wild-type	$(1.2 \pm 0.1) \times 10^{-5}$	16 ± 1 h	$(1.3 \pm 0.0) \times 10^{8}$	$(9.2 \pm 0.5) \times 10^{-14}$	3.2	
K40G	Y434A	$(9.3 \pm 0.5) \times 10^{-4}$	12 ± 1 min	$(3.1 \pm 0.2) \times 10^{7}$	$(3.0 \pm 0.2) \times 10^{-11}$	6.6	−0.2
K40G	D435A	$(1.9 \pm 0.1) \times 10^{-5}$	10 ± 1 h	$(4.7 \pm 0.1) \times 10^{7}$	$(4.0 \pm 0.2) \times 10^{-13}$	4.1	2.6
K40G	Y437A	$(5.6 \pm 0.1) \times 10^{-4}$	21 ± 1 min	$(2.7 \pm 0.6) \times 10^{7}$	$(2.1 \pm 0.5) \times 10^{-11}$	6.4	−2.4
K40G	Y434A/D435A	$(1.9 \pm 0.2) \times 10^{-3}$	6.2 ± 0.3 min	$(1.4 \pm 0.1) \times 10^{8}$	$(1.4 \pm 0.1) \times 10^{-11}$	6.2	3.8
K40G	Y434A/Y437A	$(1.9 \pm 0.1) \times 10^{-2}$	36 ± 1 s	$(1.0 \pm 0.1) \times 10^{7}$	$(1.9 \pm 0.1) \times 10^{-9}$	9.1	−1.8

[a] Kinetic parameters were determined as described in Experimental Procedures. Values for the wild-type complex are listed in Table 2. The half-life ($t_{1/2}$) for dissociation of the wild-type complex is 73 ± 14 days. $\Delta\Delta G$ values for the complexes of wild-type Ang with hRI variants Y434A, D435A, and Y437A and for wild-type hRI with R5A-Ang are listed in Table 1. [b] The standard error in $\Delta\Delta G$ for the complex of R5A-Ang with Y434A/Y437A-hRI is 0.2 kcal/mol; standard errors for all other complexes are ≤0.1 kcal/mol. [c] Standard errors for all $\Delta\Delta\Delta G$ values are ≤0.2 kcal/mol.

proximate K_i value for the Y434A/D435A-hRI·Ang complex obtained by fluorimetric examination of competition between Ang and RNase A (see Experimental Procedures) is consistent with the k_a value calculated from the faster phase. This experiment indicated that Ang binds 100−200-fold more tightly than RNase A (i.e., with a K_i of 28−56 pM). (A more precise determination could not be performed because of technical limitations.) Together with the value for k_d measured above, this sets k_a to $4.8-9.6 \times 10^7$ M^{-1} s^{-1}.

The k_a values for the Ang complexes with Y434A/D435A and Y434A/Y437A based on the more rapid process were 7.0×10^7 and 5.9×10^7 M^{-1} s^{-1}, respectively, several-fold lower than for the wild-type complex. These changes in association are much smaller than the effects on dissociation, as has generally been the case with mutations that substantially weaken protein−protein interactions (*19*, *34*, *35*). The calculated K_i value for the Y434A/D435A complex (39 pM) is equivalent to that predicted if the effects of the mutations at positions 434 and 435 are completely additive ($\Delta\Delta\Delta G = 0$). However, the K_i for the Y434A/Y437A complex (29 pM) is 74-fold higher than expected for simple additivity; i.e., the effects of the replacements at positions 434 and 437 are markedly superadditive, with $\Delta\Delta\Delta G$ being equal to −2.5 kcal/mol. Both findings stand in stark contrast to the strong subadditivities observed with the RNase A complexes. Consequently, the impacts of each double mutation on Ang and RNase A binding are nearly the same, although the single replacements at positions 434 and 437 reduced the affinity for RNase A to a much greater extent than that for Ang.

Interactions of Ang Variants R5A and K40G with hRI Single and Double Mutants. hRI Trp438 interacts with Ang primarily through its main chain, whose oxygen atom forms two H-bonds with the guanidino group of Arg5. Therefore, additivities involving the interactions of this residue were assessed through the use of R5A-Ang. Dissociation of all R5A complexes was rapid enough to measure by the fluorescence method; for the complex with Y434A/D435A-hRI, it was so fast that it could be followed only with the stopped-flow instrument. Association was monitored as for the complexes with wild-type Ang, except that a single concentration of R5A-Ang, well below K_1, was used; in the one instance where the fluorescence increase was biphasic (with Y434A/Y437A), the k_a value was calculated from the faster process, as described above.

The effects of replacing Ang Arg5 and Tyr434, Asp435, or both on hRI were all superadditive, with $\Delta\Delta\Delta G$ values ranging from −0.9 to −1.4 kcal/mol (Table 4). The impact of the three simultaneous replacements was particularly dramatic; the K_i for the triple mutant complex was 10 nM, i.e., (2.7×10^7)-fold higher than for the wild type, and the $t_{1/2}$ for dissociation was only 1.1 s. The effects of substituting Arg5 and both Tyr434 and Tyr437 were even more strongly superadditive ($\Delta\Delta\Delta G = -2.1$ kcal/mol), although the K_i value for this complex was somewhat lower, 0.7 nM.

The Ang variant K40G was used to investigate further the interactions of Lys40 with Asp435 and Tyr434 of hRI as well as to assess additional interrelationships within this interface region. The K40G complexes were characterized in the same manner as those of R5A-Ang; association was biphasic except with Y434A/Y437A. A previous study in which K40G was used (*19*) had measured k_d, but not k_a, for the complex with wild-type hRI. The missing parameter was now determined so that the K_i value for this complex could be calculated. The resultant $\Delta\Delta G$ value, 3.2 kcal/mol (Table 4), was similar to that produced by Ala substitution of Asp435, the H-bonding partner of Lys40 (3.5 kcal/mol). The $\Delta\Delta G$ values for replacing Lys40 and Asp435 within the context of the Ang·Y434A-hRI complex also agreed closely (3.3 and 3.5 kcal/mol, respectively). Replacement of Lys40 in the Ang·D435A-hRI complex produced only a small additional effect (0.6 kcal/mol), and substitution of this residue in the Ang·Y434A/D435A-hRI complex in fact increased affinity slightly (by 0.4 kcal/mol). Thus, the effects of replacing Ang Lys40 and hRI Asp435 are almost entirely nonadditive, whereas those of substituting Lys40 and hRI Tyr434 are fully additive, as for the combination of residues 434 and 435 (Table 3).

In contrast, replacing Ang Lys40 together with hRI Tyr437 revealed strong superadditivity ($\Delta\Delta\Delta G = -2.4$ kcal/mol), similar to that measured for the complex of Ang with Y434A/Y437A-hRI. A somewhat smaller superadditivity ($\Delta\Delta\Delta G = -1.8$ kcal/mol) was observed when all three mutations were incorporated. The K_i for binding of K40G-Ang to Y434A/Y437A-hRI (1.9 nM) was the second highest for any of the complexes that were examined, as was the k_d value. Association was 28-fold slower than for the wild-type complex, by far the largest change observed for this parameter.

DISCUSSION

Nature of the Hot Spot in the hRI·RNase A Binding Interface. The results of earlier mutational studies showed that the region of the hRI·RNase A interface containing hRI residues Tyr434, Asp435, Tyr437, and Ser460 constitutes an energetic hot spot (*19*). Residues 434, 435, and 437 lie on a single loop, with Ser460 juxtaposed next to them in the three-dimensional structure; this cluster blocks the active center of RNase A, contacting the P_1 catalytic site (Lys41 and His119), B_2 purine-binding subsite (Gln69, Asn71, Ala109, and Glu111), and the P_2 phosphate-binding subsite (Lys7) (the subsite nomenclature is from ref *36*). Individual mutations of these hRI residues decreased the binding energy by 2.6−5.9 kcal/mol. Substitutions of five others (Glu287, Lys320, Glu401, Cys408, and Arg457) produced much smaller changes, although all of these amino acids form H-bonds or salt bridges in the crystal structure. Deletion of the internal segment of residues 315−371, which eliminates the interactions of all 10 contact residues between the N-terminus and residue 371 because of the horseshoe shape of the inhibitor, increased K_i only by 630-fold (*29*). None of the nine contact residues on hRI still to be investigated interact extensively with RNase A in the crystal structure of the complex, and only one forms an H-bond. Six of them are neighbors of residues 434−437 and/or 460 that may also contribute to the hot spot.

The mutagenesis results indicated that Tyr434 is the hRI residue most important for binding RNase A. However, the nature of its role is not obvious from the crystal structure. The H-bond between the Tyr OH group and the carbonyl O of RNase A Leu35 appears to be weak (donor−acceptor distance of 3.4 Å), and this is now supported by the finding that Y434F-hRI is functionally indistinguishable from the wild-type inhibitor (Table 2). The phenyl ring of Tyr434 forms numerous van der Waals contacts with RNase A and becomes almost completely buried in the complex [solvent-accessible surface area (ASA) decreases from 73 to 6 Å^2]. In principle, these contacts and the hydrophobic effect might provide appreciable binding energy. However, elimination of the phenyl group of Tyr437, which forms nearly as many interactions and undergoes a still larger decrease in ASA (from 102 Å^2 in free RI to 6 Å^2 in the complex), had only a minor effect; $\Delta\Delta G$ for Phe437 → Ala is 0.5 kcal/mol, i.e., 5.3 kcal/mol smaller than that for Phe434 → Ala (Table 2). Moreover, the burying of Tyr434 in the interface appears to have an energetic cost; it requires an ∼180° rotation of the side chain of Arg39, whose positions in the structures of free RNase A and RNase−nucleotide complexes conflict with that occupied by Tyr434 in the RI complex (*16*).

Results obtained in this study with Y434A/D435A-hRI and Y434A/Y437A-hRI suggest that in fact much of the contribution of Tyr434 to binding of RNase A is indirect. The losses in binding energy for both double mutations are strongly subadditive, implying that Tyr434 is functionally coupled to Asp435 and Tyr437 in the complex. One plausible basis for this would be that removal of the Tyr434 side chain attenuates the interactions of the other residues. In this case, the portion of $\Delta\Delta G$ for Y434A-hRI that is attributable to indirect effects on Asp435 and Tyr437 could be as high as 63% (3.7 kcal/mol), since $\Delta\Delta G$ values for replacement of Asp435 in wild-type and Y434A-hRI differ by 2.4 kcal/mol and $\Delta\Delta G$ values for replacement of Tyr437 in these two RIs differ by 1.3 kcal/mol.

An alternative or additional basis for the observed couplings would be that substitutions of Asp435 and Tyr437 each impair the interactions of Tyr434. This would imply that the direct energetic contributions of Asp435 and Tyr437 are much smaller than the $\Delta\Delta G$ values measured for the Ala variants. Although this possibility cannot be excluded, we note that the changes in binding energy produced by replacing residues 435 and 437 are more readily understandable than that engendered by mutating residue 434. The $\Delta\Delta G$ value for D435A-hRI (3.6 kcal/mol) is reasonable for the loss of the putative H-bonds with Lys41; indeed, the similar effect of mutating Asp435 in the hRI·Ang complex seems to be almost entirely due to disruption of the corresponding interactions (see below). The $\Delta\Delta G$ values for removal of the Tyr437 OH and phenyl groups are 2.1 and 0.5 kcal/mol, respectively. The first of these values is not excessive for the loss of the two H-bonds of the OH moiety, both of which are well-buried and one of which is short (donor−acceptor distance of 2.7 Å). The second value is low, rather than high, in view of the 10 van der Waals contacts and extensive burying of the phenyl ring in the complex. The preceding considerations also argue against another potential explanation for the subadditive effects of the mutations of the 434 and 435 and 434 and 437 pairs, i.e., that the replacement pairs have common negative effects on solvent structure or on energetically significant interactions of other residues. Moreover, thermal denaturation studies have shown that Ala substitutions of Tyr434 and Asp435 do not perturb the overall hRI structure (*19*).

Functional coupling between Tyr434 and Asp435 is not surprising given the short distance (5.7 Å) separating these residues and the contact residue on RNase, Lys41, that they share. Tyr434 might strengthen the 435−41 H-bonds by aligning the two residues optimally and/or by shielding them from solvent. The conformational change in RNase A associated with binding of Tyr434 might also help to improve these bonds. It is more difficult to envision how Tyr434 is linked to Tyr437, as these residues are 13 Å apart, and their contacts on RNase A approach no closer than ∼7 Å (the major Tyr434 contact, Lys41, is separated from the Tyr437 H-bonding partners Asn71 and Glu111 by even greater distances, 16−18 Å). Perhaps the loss of the side chain of residue 434 alters the local RI backbone structure in a manner that propagates to residue 437, which is on the same loop.

The pRI·RNase A crystal structure indicates ways in which Tyr434 might influence interactions of RI residues Glu401 and Ser460 as well. The two H-bonds between Glu401 and Arg39 of RNase A are able to form only because of the movement of the Arg side chain facilitated or induced by Tyr434; elimination of these H-bonds by Ala substitution of Glu401 decreases the complex stability by 1.3 kcal/mol (unpublished data). van der Waals contacts of Tyr434 with Ser460 might help to optimize the H-bonds of the Ser with Lys7 and Gln11 of RNase A; removal of the Ser460 interactions produces a $\Delta\Delta G$ value of 3.5 kcal/mol (*19*).

In summary, the present findings suggest that Tyr434 serves as a key linchpin that functions largely by enhancing interactions of other residues within, and possibly beyond, the hot spot region of the hRI·RNase A interface rather than by forming strong direct contacts of its own. A more detailed

understanding of the elaborate role of this residue—and, indeed, confirmation of this hypothesis—must await the outcome of further mutational and crystallographic studies. Nonetheless, it is already clear that the residues within the hot spot of the RI·RNase A interface do not function independently and that the effects of single-residue mutations overestimate the contributions of some or all of these amino acids.

Nature of the Hot Spot in the hRI·Ang Binding Interface. As with the RNase A complex, mutagenesis results point to the existence of a hot spot in the hRI·Ang interface encompassing loop residues 434−438 and its neighbor residue 460 on hRI and the $P_1/B_2/P_2$ portion of the enzyme active site. Replacements of four amino acids in this region (hRI Tyr434 and Asp435 and Ang Arg5 and Lys40) increased K_i substantially ($\Delta\Delta G = 2.3-4.2$ kcal/mol), and substitutions of four others (hRI Tyr437 and Ser460 and Ang His8 and His114) produced smaller, but significant, changes ($\Delta\Delta G = 0.6-1.3$ kcal/mol). Replacements of three Ang residues (Arg31, Arg32, and Trp89) that form H-bonds and extensive van der Waals contacts with hRI in other parts of the interface had little or no impact. Indeed, the results of preliminary single-site mutagenesis studies on the remainder of the interface suggest that no residues outside the key region already identified make large energetic contributions (R. Shapiro, unpublished).

Most of the effects of single-site substitutions within the hot spot are readily understandable from the crystal structure of the hRI·Ang complex. Replacements of hRI Asp435 and Ang Lys40, residues which are linked by two well-buried, medium-length H-bonds and three van der Waals interactions, decrease the binding free energy by 3.5 and 3.2−4.2 kcal/mol, respectively (Tables 1 and 4). Although each of these amino acids forms additional intermolecular interactions (Asp435 with Gln117 directly and with Asp41 and Leu115 via water; Lys40 with Tyr434), the present findings suggest that only their contacts with each other are energetically important. (i) $\Delta\Delta G$ values for Asp435 → Ala and Lys40 → Gly are nearly identical; (ii) the effects of replacing Asp435 and Lys40 are almost entirely nonadditive, and (iii) the effects of mutating Lys40 and Tyr434 are fully additive. Substitution of Ang Arg5 by Ala decreases the binding energy by 2.3 kcal/mol; this residue forms two H-bonds with Trp438 of hRI, a water-mediated H-bond with Ile436, and van der Waals contacts with Trp438, Ser439, and Glu440. Presumably, the strongest of these interactions are the direct H-bonds, although neither is optimal; one is well-buried but long, and the other is short but only partially buried. Replacement of hRI Tyr437 by Ala produces a relatively minor change in affinity ($\Delta\Delta G = 0.8$ kcal/mol), and mutation to Phe has no effect (Table 2). This is again consistent with the crystal structure, where Tyr437 makes a small number of van der Waals contacts with Ala106, Glu108, and His114 of Ang and does not form any H-bonds. Deletion of hRI Ser460, which eliminates the H-bonds of this residue with His8 and Gln12 of Ang, yields a $\Delta\Delta G$ value of 1.3 kcal/mol.

The basis for the 3.3 kcal/mol loss in binding energy that results from mutating hRI Tyr434 to Ala is less evident from the crystal structure. The phenyl group of this residue forms several van der Waals contacts with the alkyl portion of Ang Lys40 and becomes almost fully buried upon complex formation. As just noted, the effects of replacing Tyr434 and Lys40 are entirely independent, suggesting that the interactions between these two amino acids do not make an important contribution. Nonetheless, the hydrophobic effect still might account for much of the reduced affinity of Y434A-hRI for Ang; i.e., it is possible that removal of the Lys40 side chain does not increase significantly the accessibility of the Tyr434 phenyl group to solvent. In addition, the $\Delta\Delta G$ value of 0.6 kcal/mol for replacement of Tyr434 by Phe (Table 2) suggests that the OH group of the tyrosine may form a weak H-bond not observed in the X-ray structure, where its oxygen atom is 3.7 Å from the nearest potential partner (Pro38 O). It is also possible that the phenyl group forms a more favorable set of interactions under the conditions used for the kinetic experiments than it does in the crystal. [We note, however, that the complex is extremely stable ($t_{1/2} \approx 70$ days) in solution under the crystallization conditions (*14*).] In addition, Tyr434 might provide binding energy by altering the arrangement of the solvent at the protein surfaces; this is particularly difficult to assess because the structure of free hRI has not been determined.

Tyr434 does not appear to contribute to binding of Ang via the indirect mechanism proposed for it in the RNase A complex. The effects of replacing this residue and Asp435 are completely additive, and the effects of mutating it together with hRI Tyr437 and/or Ang Arg5 are superadditive. The simplest interpretation of these findings is that Tyr434 and Asp435 are functionally independent and that replacement of Tyr434 does not reduce (and might increase; see below) the contributions of Tyr437 and Arg5. These additivities also provide further evidence that the loss of the side chain of residue 434 does not cause any general perturbation of the inhibitor structure. However, we cannot exclude the possibility that the Tyr434 substitution attenuates specific interactions of residues other than those examined here. For example, removal of the two short (3.2 and 3.4 Å) van der Waals contacts of the residue 434 phenyl ring with Ser460 CB might affect the H-bonds of residue 460 OG with His8 and Gln12 of Ang.

Superadditive mutational effects are found whenever hRI Tyr437 or Ang Arg5 is replaced together with the other residues that have been examined (Tables 3 and 4). They are particularly large for the combinations of Tyr437 with Tyr434 and with Ang Lys40, which give $\Delta\Delta\Delta G$ values of −2.5 and −2.4 kcal/mol, respectively. $\Delta\Delta\Delta G$ values for replacements of Arg5 and Tyr434, Asp435, or both are smaller (−0.9 to −1.4 kcal/mol). The superadditivities associated with mutations of Arg5 and Tyr437 do not seem to be independent, as $\Delta\Delta\Delta G$ for the 434, 437, 5 triple combination is about the same as for the 434 and 437 pair by itself. These findings suggest that the hot spot residues fall into two groups, Tyr434, Asp435, and Lys40 and Tyr437 and Arg5; the effects of eliminating multiple interactions within each group are additive, whereas mutations involving both groups give superadditive effects. All of the superadditivities measured are highly significant since the errors in the $\Delta\Delta\Delta G$ values are in the range of 0.1−0.2 kcal/mol. Moreover, the effects would be even larger if our decision to calculate k_a values for biphasic associations from the faster, rather than the slower, process was incorrect.

One potential physical basis for the observed superadditivities is that replacement of one residue within the pair or

group strengthens the contacts of others. For example, once the side chain of hRI Tyr437 or Ang Arg5 is removed, hRI Tyr434 and Ang Lys40 might form more effective interactions with each other, and the Asp435···Lys40 H-bonds might also be improved; this would imply that the actual energetic contributions of Tyr437 and Arg5 in the wild-type complex are larger than the effects of single-site mutations. Conversely, losses of the Tyr434 and Lys40 side chains might enhance the contacts of Tyr437, allowing this residue to pack better or to form a strong H-bond with Glu108 (the residue 437 OH and residue 108 OE2 are slightly beyond H-bonding distance in the wild-type complex), or perhaps to engage in a cation−π interaction (*37*) with His114; this would imply that the free energy losses for the individual Tyr434 and Lys40 replacements underestimate the true importance of these residues in the wild-type complex. Similarly, substitutions of Tyr434 and Lys40 might serve to strengthen the H-bonds of Ang Arg5 with Trp438 of hRI. This type of negative cooperativity might reflect the difficulty of optimizing multiple interactions simultaneously when the evolutionary driving force is not only to maximize affinity but also to maintain broad specificity (hRI must bind tightly to all members of the RNase superfamily; see ref *38*).

An alternative explanation for superadditivity is that the loss of the interactions of one residue is offset by the formation of entirely new interactions by other residues within the group. This would require at least some localized structural rearrangements of hRI, Ang, or both. In this regard, it should be noted that the loop that contains residues 434−438 makes relatively few interactions with other structural elements on hRI and therefore might be quite flexible. This mechanism of superadditivity would again imply that some of the interactions in this region make greater contributions than is apparent from the single-residue replacements.

In principle, superadditive effects could also result if multiresidue substitutions weaken or disrupt the interactions of other residues but the individual replacements do not. In this case, the basis for the observed superadditivities in fact would be similar to that proposed above for the subadditivities in the RNase A complex. Although this possibility cannot be ruled out entirely, it seems unlikely because $\Delta\Delta\Delta G$ values for the triple mutations of Tyr434, Asp435, and Arg5, Tyr434, Tyr437, and Arg5, and Tyr434, Tyr437, and Lys40 are all similar to or greater than those for any of the double mutations.

In light of these considerations, we conclude that the hot spot in the hRI·Ang interface plays an even more critical role than had been suggested by earlier studies with single-residue variants. Elimination of the interactions of only three of the residues in this site (Tyr434, Asp435, and Arg5) together decreases the binding free energy by 10.1 kcal/mol (47% of the total). Replacement of a fourth residue, Tyr437, would be expected to have a significant further effect since in all variant and variant·variant complexes examined this substitution reduced the binding energy by >1.5 kcal/mol. The interactions of Ser460 might also add to the overall contribution of this region; the $\Delta\Delta G$ value for deletion of this residue in the wild-type complex is 1.3 kcal/mol, and the results of preliminary studies (R. Shapiro, unpublished) indicate that the energy losses for double mutations involving Ser460 are superadditive.

Implications for Protein−Protein Interactions in General. Single-site mutagenesis has been used extensively to investigate the distribution of binding free energy within protein−protein interfaces. Although the maps obtained, in conjunction with the corresponding crystal structures, provide critical information on the molecular basis for binding affinity, they do not reveal how the whole is generated from its parts. This issue is commonly addressed, as it is in this study, by replacing two or more residues both separately and together and comparing the effects that are produced (*39*−*41*). If the $\Delta\Delta G$ value for the multiple mutation equals the sum of those for the individual mutations [i.e., if $\Delta\Delta\Delta G$ (sometimes termed "$\Delta\Delta G_{int}$") is zero], this suggests that the residues are functionally independent. Positive $\Delta\Delta\Delta G$ values obtained when two residues on the different protein partners are replaced are taken to be quantitative measures of the energy of the interaction between the residues as long as the mutations have not produced secondary effects, e.g., on protein or solvent structure. Although such complications can be ignored in many cases, there are numerous examples where they clearly come into play since significantly positive $\Delta\Delta G$ values (i.e., subadditivities) are measured for residues that form no direct pairwise or triangulated contacts (*20*, *42*, *43*).

Early studies in which multiple sites were mutated on the same protein partner showed the effects to be fully additive as a rule (*44*, *45*). However, many instances of subadditivity have now been documented (*46*, *47*). Indeed, this phenomenon must be quite prevalent because the sum of $\Delta\Delta G$ values for single-residue mutants is much greater than the ΔG value for virtually all complexes that have been examined; in the most striking cases, $\Sigma\Delta\Delta G$ and ΔG differ by nearly a factor of 4 (*48*, *49*). The subadditivities observed previously have generally involved interface residues that are neighbors, and can often be explained qualitatively in terms of intramolecular contacts. The effect of the hRI Tyr434/Asp435 double replacement on the affinity for RNase A reported here constitutes yet another example of this situation. In contrast, the coupling between the hRI Tyr434 and Tyr437 side chains in binding RNase A occurs over a distance of >13 Å and does not seem to reflect any direct or mediated interactions. The paucity of analogous cases in the literature probably reflects the limited extent to which studies on protein−protein complexes have examined interrelationships between distant residues on the same protein, as compared to those on the two interacting proteins. This type of long-range thermodynamic coupling within proteins has been seen for both protein folding (*50*) and enzymatic systems (see refs *20* and *51*).

Superadditive mutational effects such as those observed here for the hRI·Ang complex seem to be much rarer. Indeed, we are not aware of any reported previously that are strictly comparable. Jin and Wells (*47*) found that the affinity decreases produced by Ala replacements of key antibody-binding determinants on human growth hormone became 4−20-fold greater when groups of five to nine neighboring residues were also mutated to Ala (i.e., $\Delta\Delta\Delta G$ values ranged from −0.8 to −1.8 kcal/mol). These superadditivities differ from those measured in this study in that they involve larger sets of mutations and can potentially be explained by the close proximity of the various replacement sites. The most substantial $\Delta\Delta\Delta G$ values for the hRI·Ang complex were obtained for the double mutations 434(hRI)/437(hRI) and

437(hRI)/40(Ang); these side chain pairs are separated by at least 13.6 and 13.4 Å, respectively (the shortest distances between the two residues; CG−CG and CG−NZ, respectively), and there are no apparent links between them other than the main chain. The 434(hRI)/5(Ang) combination gives a somewhat smaller $\Delta\Delta\Delta G$ value for residues that are similarly separated (>12.6 Å; CG−NH2). Outside of protein−protein complexes, superadditivities have been seen in protein folding and enzymatic systems (compiled in refs *20* and *51*), but these are likely to have very different physical meanings.

The same types of secondary physicochemical effects of mutations that are usually invoked to account for subadditivity can also apply to superadditivity. These include changes in local or global protein conformation, solvent structure, electrostatic fields or dielectric constants, and protein dynamic properties. However, whereas subadditivity for protein−protein complexes reflects the fragility of the specific intermolecular interactions (i.e., how easily the loss of one interaction can impact on others), superadditivity reflects the plasticity and adaptability of the interface (i.e., how readily the interactions lost can be compensated for). Clearly, this latter property is particularly beneficial when one protein component must evolve to recognize multiple ligands of diverse structure as in the RI−RNase/Ang system, where the sequences of the targets are only ∼25−35% identical. Nonetheless, it seems likely that detailed studies of additional protein−protein complexes will reveal that superadditivity has been widely utilized in nature.

Nonadditivity has enormous implications for the interpretation of binding energy hot spots identified by single-site mutagenesis. As seen for the two hRI complexes, such sites can be either "hotter" or "less hot" than they appear. In the examples presented here, the binding energy within the key region was overestimated due to subadditivity and underestimated as a result of superadditivity. However, each type of nonadditivity can have the opposite outcome as well. If some residues function largely to support the hot spot, as proposed for the complex of human growth hormone with its receptor, then the effects of mutating them together with the critical amino acids will be subadditive, and this would now mean that the binding energy is in reality more focused than it appeared from the single-residue replacements (*52*). If the effects of mutating combinations of non-hot spot residues are superadditive, this would indicate that these residues are more important (and the interaction energy less concentrated) than they seemed to be on the basis of the individual substitutions.

The extent to which binding free energy is localized within hot spots has obvious ramifications for the design of small molecules that block or mimic protein−protein interfaces; in general, the more concentrated the energy is, the more likely it is that these agents can be developed. Indeed, in cases where the critical region comprises a single small segment, it may be possible to utilize this peptide directly if appropriate constraints can be introduced to achieve the correct conformation. At the same time, complex interrelationships among the crucial residues, such as those observed for the hRI interactions, might make this task more difficult even when the key site is very compact. If residues exhibit positive cooperativity (i.e., if mutational effects are subadditive), then subtle deviations from optimal positioning for a single amino acid can weaken multiple interactions and thereby decrease affinity dramatically. If negative cooperativity exists (i.e., if mutational effects are superadditive), then it might be extremely challenging to maintain strong interactions of multiple residues simultaneously. Moreover, caution must be exercised when deciding which elements of the hot spot region to incorporate into the designed molecule. A residue that is dispensable in one context may be extremely important in another that differs only slightly; e.g., Tyr437 appears to make a much larger contribution to binding Ang as part of Y434A than as part of wild-type hRI. However, it might also be possible to exploit negative cooperativity to increase affinity, if methods can be devised for uncoupling the various residues so that they can all fulfill their full binding potential in the presence of the others.

ACKNOWLEDGMENT

We thank Melisa Ruiz-Gutierrez for excellent technical assistance, Drs. A. C. Papageorgiou and K. R. Acharya for panels B and C of Figure 1, Drs. K. R. Acharya, J. F. Riordan, and D. S. Auld for helpful advice and discussions, Dr. E. A. Fox for initial studies on the interaction of W89M-Ang with hRI, and Dr. D. J. Strydom for amino acid analyses.

REFERENCES

1. Janin, J. (1995) *Prog. Biophys. Mol. Biol. 64*, 145−166.
2. Wells, J. A. (1996) *Proc. Natl. Acad. Sci U.S.A. 93*, 1−6.
3. Jones, S., and Thornton, J. M. (1996) *Proc. Natl. Acad. Sci. U.S.A. 93*, 13−20.
4. Braden, B. C., Goldman, E. R., Mariuzza, R. A., and Poljak, R. J. (1998) *Immunol. Rev. 163*, 45−57.
5. Bogan, A. A., and Thorn, K. S. (1998) *J. Mol. Biol. 280*, 1−9.
6. Clackson, T., and Wells, J. A. (1995) *Science 267*, 383−386.
7. Fett, J. W., Strydom, D. J., Lobb, R. R., Alderman, E. M., Bethune, J. L., Riordan, J. F., and Vallee, B. L. (1985) *Biochemistry 24*, 5480−5486.
8. Shapiro, R., Riordan, J. F., and Vallee, B. L. (1986) *Biochemistry 25*, 3527−3532.
9. Lee, F. S., Shapiro, R., and Vallee, B. L. (1989) *Biochemistry 28*, 225−230.
10. Olson, K. A., Fett, J. W., French, T. C., Key, M. E., and Vallee, B. L. (1995) *Proc. Natl. Acad. Sci. U.S.A. 92*, 442−446.
11. Olson, K. A., and Fett, J. W. (1996) *Proc. Am. Assoc. Cancer Res. 37*, 57.
12. Shapiro, R., and Vallee, B. L. (1987) *Proc. Natl. Acad. Sci. U.S.A. 84*, 2238−2241.
13. Polakowski, I. J., Lewis, M. K., Muthukkaruppan, V. R., Erdman, B., Kubai, L., and Auerbach, R. (1993) *Am. J. Pathol. 143*, 507−517.
14. Papageorgiou, A. C., Shapiro, R., and Acharya, K. R. (1997) *EMBO J. 16*, 5162−5177.
15. Kobe, B., and Deisenhofer, J. (1995) *Nature 374*, 183−186.
16. Kobe, B., and Deisenhofer, J. (1996) *J. Mol. Biol. 264*, 1028−1043.
17. Lee, F. S., and Vallee, B. L. (1989) *Biochemistry 28*, 3556−3561.
18. Shapiro, R., and Vallee, B. L. (1992) *Biochemistry 31*, 12477−12485.
19. Chen, C. Z., and Shapiro, R. (1997) *Proc. Natl. Acad. Sci. U.S.A. 94*, 1761−1766.
20. LiCata, V. J., and Ackers, G. K. (1995) *Biochemistry 34*, 3133−3139.
21. Lee, F. S., and Vallee, B. L. (1989) *Biochem. Biophys. Res. Commun. 160*, 115−120.
22. Fett, J. W., Olson, K. A., and Rybak, S. M. (1994) *Biochemistry 33*, 5421−5427.
23. Shapiro, R., Fox, E. A., and Riordan, J. F. (1989) *Biochemistry 28*, 1726−1732.
24. Blackburn, P., Wilson, G., and Moore, S. (1977) *J. Biol. Chem. 252*, 5904−5910.

25. Sela, M., and Anfinsen, C. B. (1957) *Biochim. Biophys. Acta 24*, 229−235.
26. Lee, F. S., Auld, D. S., and Vallee, B. L. (1989) *Biochemistry 28*, 219−224.
27. Ho, S. N., Hunt, H. D., Horton, R. M., Pullen, J. K., and Pease, L. R. (1989) *Gene 77*, 51−59.
28. Lee, F. S., Fox, E. A., Zhou, H. M., Strydom, D. J., and Vallee, B. L. (1988) *Biochemistry 27*, 8545−8553.
29. Lee, F. S., and Vallee, B. L. (1990) *Biochemistry 29*, 6633−6638.
30. Witzel, H., and Barnard, E. A. (1962) *Biochem. Biophys. Res. Commun. 7*, 295−299.
31. Vicentini, A. M., Kieffer, B., Matthies, R., Meyhack, B., Hemmings, B. A., Stone, S. R., and Hofsteenge, J. (1990) *Biochemistry 29*, 8827−8834.
32. Hofsteenge, J., Kieffer, B., Matthies, R., Hemmings, B. A., and Stone, S. R. (1988) *Biochemistry 27*, 8537−8544.
33. Wlodawer, A., Svensson, L. A., Sjolin, L., and Gilliland, G. L. (1988) *Biochemistry 27*, 2705−2717.
34. Schreiber, G., and Fersht, A. R. (1993) *Biochemistry 32*, 5145−5150.
35. Cunningham, B. C., and Wells, J. A. (1993) *J. Mol. Biol. 234*, 554−563.
36. Richards, F. M., and Wyckoff, H. W. (1973) in *The Atlas of Molecular Structures in Biology* (Phillips, D. C., and Richards, F. M., Eds.) Clarendon Press, Oxford, U.K.
37. Dougherty, D. A. (1996) *Science 271*, 163−168.
38. Shapiro, R., Riordan, J. F., and Vallee, B. L. (1995) *Nat. Struct. Biol. 2*, 350−354.
39. Carter, P. J., Winter, G., Wilkinson, A. J., and Fersht, A. R. (1984) *Cell 38*, 835−840.
40. Ackers, G. K., and Smith, F. R. (1985) *Annu. Rev. Biochem. 54*, 597−629.
41. Horovitz, A. (1987) *J. Mol. Biol. 196*, 733−735.
42. Schreiber, G., and Fersht, A. R. (1995) *J. Mol. Biol. 248*, 478−486.
43. Goldman, E. R., Dall'Acqua, W., Braden, B. C., and Mariuzza, R. A. (1997) *Biochemistry 36*, 49−56.
44. Wells, J. A. (1990) *Biochemistry 29*, 8509−8517.
45. Cunningham, B. C., and Wells, J. A. (1991) *Proc. Natl. Acad. Sci. U.S.A. 88*, 3407−3411.
46. Kelley, R. F., and O'Connell, M. P. (1993) *Biochemistry 32*, 6828−6835.
47. Jin, L., and Wells, J. A. (1994) *Protein Sci. 3*, 2351−2357.
48. Dall'Acqua, W., Goldman, E. R., Eisenstein, E., and Mariuzza, R. A. (1996) *Biochemistry 35*, 9667−9676.
49. Muller, Y. A., Chen, Y., Christinger, H. W., Li, B., Cunningham, B. C., Lowman, H. B., and de Vos, A. M. (1998) *Structure 6*, 1153−1167.
50. Green, S. M., and Shortle, D. (1993) *Biochemistry 32*, 10131−10139.
51. Mildvan, A. S., Weber, D. J., and Kuliopulos, A. (1992) *Arch. Biochem. Biophys. 294*, 327−340.
52. Clackson, T., Ultsch, M. H., Wells, J. A., and de Vos, A. M. (1998) *J. Mol. Biol. 277*, 1111−1128.
53. Kraulis, P. J. (1991) *J. Appl. Crystallogr. 24*, 946−950.

BI990762A